Singular optical manipulation of birefringent elastic media using nonsingular beams

Etienne Brasselet

Centre de Physique Moléculaire Optique et Hertzienne, Université Bordeaux 1, CNRS, 33405 Talence Cedex, France (e.brasselet@cpmoh.u-bordeaux1.fr)

Received June 24, 2009; revised September 18, 2009; accepted September 21, 2009; posted September 23, 2009 (Doc. ID 113151); published October 15, 2009

It is shown that nonsingular light beams can generate singular birefringent patterns in homogeneous birefringent elastic media. These orientational defects of the optical-axis spatial distribution originate from an optical torque driven by a nonzero longitudinal field component. Singular radial and spin-dependent azimuthal light-induced elastic distortion patterns are described and experimentally observed in a uniform liquid-crystal film in the course of a focused circularly polarized Gaussian beam. © 2009 Optical Society of America

OCIS codes: 260.1440, 160.1190.

Light fields can possess and propagate angular momentum, sum of a spin and an orbital contribution [1] that may be coupled. Such coupling can appear as much at the interface between two isotropic media [2], in inhomogeneous locally isotropic media [3], or during scattering by an isotropic particle [4], as in homogeneous [5,6] or inhomogeneous [7–9] anisotropic media. The most promising spin-to-orbital angular-momentum couplers are based on nonreconfigurable axially symmetric spatially patterned birefringent liquid-crystal (LC) elements [8,10,11]. Here we show the possibility to optically induce singular birefringent patterns in the bulk of initially homogeneous and uniform birefringent elastic media from light fields free from any singular structure. We develop a model for the most common birefringent and elastic media—liquid crystals—and experimental demonstration is reported.

Let us consider a homogeneous slab of a uniaxial medium lying in the (x,y) plane, with its optical axis $\mathbf{n}$ along z, in the course of a normally incident light beam. An optical torque density $\boldsymbol{\Gamma} \propto \epsilon_a(\mathbf{n}\times\mathbf{E}^*)(\mathbf{n}\cdot\mathbf{E})$ + c.c. is therefore exerted by light on the birefringent medium, where $\mathbf{E}$ is the complex electric field, $\epsilon_a=\epsilon_\parallel-\epsilon_\perp$ is the anisotropy of the permittivity tensor ϵ_{ij}, and symbols $\perp$ ($\parallel$) refer to directions perpendicular (parallel) to $\mathbf{n}$ and c.c. to complex conjugate. Namely,

$$\boldsymbol{\Gamma} \propto \epsilon_a E_z^*(-E_\phi \mathbf{e}_r + E_r \mathbf{e}_\phi) + \text{c.c.}, \tag{1}$$

where $(\mathbf{e}_r,\mathbf{e}_\phi,\mathbf{e}_z)$ is the cylindrical coordinates basis. Obviously, a plane-wave light–matter interaction implies no torque, since $E_z=0$ in that case. However, a focused light beam exerts nonzero radial ($\boldsymbol{\Gamma}_r$) and azimuthal ($\boldsymbol{\Gamma}_\phi$) torque densities owing to the existence of a longitudinal field component $E_z\neq 0$. In elastic media such as LCs, the above torques will respectively excite azimuthal ($\delta\mathbf{n}_\phi$) and radial ($\delta\mathbf{n}_r$) distortions of the optical axis spatial distribution,

$$\delta\mathbf{n} = \delta \mathrm{n}_r \mathbf{e}_r + \delta \mathrm{n}_\phi \mathbf{e}_\phi \tag{2}$$

(see Fig. 1). Note that this situation differs from the optical Fréedericksz transition problem [12], since $\boldsymbol{\Gamma}\neq 0$ for $\delta\mathbf{n}=0$, i.e., there is no threshold.

The general procedure relies on the minimization of the total free energy $\mathcal{F}=\int_0^L\int_0^\infty\int_0^{2\pi} r(F_{\text{el}}+F_{\text{opt}})\mathrm{d}\phi \mathrm{d}r \mathrm{d}z$, where $F_{\text{el,em}}$ are the elastic and optical free-energy densities, respectively (input facet at $z=0$, thickness L). Namely, $F_{\text{el}}=(1/2)K[(\nabla\cdot\mathbf{n})^2+|\nabla\times\mathbf{n}|^2]$, with K the Frank elastic constant in the single-constant approximation and $F_{\text{opt}}=-(1/16\pi)\epsilon_{ij}E_iE_j^*$. To solve the problem thus requires (i) the knowledge of the light field in the medium and (ii) an ansatz for the elastic distortions.

To tackle with the first condition we use an incident circularly polarized (CP) Gaussian beam for the purpose of illustration. The electric field inside the LC is derived within the paraxial approximation of a beam passing through a c-cut uniaxial medium [13], thus neglecting the feedback of small distortions on the light propagation itself. Then, a convenient approximate solution for the transverse part of the field is obtained from [14] and the derivation of the longitudinal part follows from [13]. We obtain, up to the phase factor $\exp(-i\omega t+ik_0n_\perp z)$,

$$\mathbf{E}_\pm = E_0 G\left[\cos\Delta\mathbf{c}_\pm + i\sin\Delta e^{\pm 2i\phi}\mathbf{c}_\mp - \frac{r}{Z\sqrt{2}}e^{\pm i\phi}\mathbf{e}_z\right], \tag{3}$$

where $\mathbf{E}_\pm$ refers to left/right-handed incident CP described by the unit vectors $\mathbf{c}_\pm=(\mathbf{e}_x\pm i\mathbf{e}_y)/\sqrt{2}$; $G=-(iz_0/Z)\exp(i\beta r^2/Z)$, with $Z=z-iz_0$, $\beta=\pi n/\lambda$, $z_0=\pi n w_0^2/\lambda$ the Rayleigh distance, $n=(n_\perp+n_\parallel)/2$ and λ

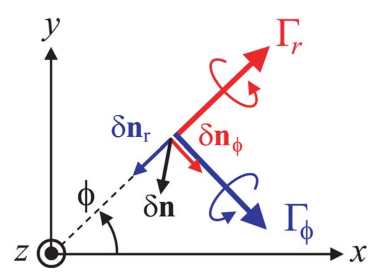

Fig. 1. (Color online) Illustration of the radial and azimuthal components of the optical dielectric torque density exerted on a c-cut optically uniaxial medium (optical axis along z).

the wavelength; and $\Delta=\epsilon\beta r^2 z/Z^2$ with $\epsilon=(n_\parallel-n_\perp)/n$. We notice that, in a first attempt, the strong focusing corrections [2,15,16] can be neglected, as justified experimentally by using an NA=0.5 objective in an underfilling configuration.

The second condition is inferred from the torque and field expressions given above, which lead us to retain a cylindrically symmetric radial dependence of the form $\delta n_\alpha \propto (r/w_0)\exp(-2r^2/w_0^2)$, with $\alpha=(r,\phi)$ that implicitly assumes an isotropic elasticity. In addition, strong boundary conditions for $\mathbf{n}$ allow us to choose $\delta n_\alpha \propto \Sigma_m A_\alpha^{(m)} \sin(mqz)$, where m are positive integers, $q=\pi/L$, for the longitudinal dependence. Distortions are therefore sought in the form

$$\delta n_\alpha(r,z) = \frac{r}{w_0}\exp(-2r^2/w_0^2)\sum_m A_\alpha^{(m)}\sin(mqz). \quad (4)$$

Following Eqs. (3) and (4), equilibrium states are found from $\partial\mathcal{F}/\partial p_k=0$ with $\mathbf{p}=(A_r^{(1)},\ldots,A_r^{(M)}, A_\phi^{(1)},\ldots,A_\phi^{(M)})$ by retaining M modes only. In the simplest monomodal description, $M=1$, the resulting matrical system of equations writes $\hat{\mathbf{M}}(A_r,A_\phi)^{\mathrm{T}}=\mathbf{V}$ with

$$M_{nn} = \frac{\pi\tilde{L}}{32}(8+\tilde{q}^2\theta_0^2) - 4\epsilon\tilde{P}\int_0^{\tilde{L}} f(\tilde{z}) \times \left[\mathcal{L}_{3,3} + (-1)^n\epsilon\frac{\tilde{4}z^2}{(1+\tilde{z}^2)^2}\mathcal{L}_{5,3}\right]\mathrm{d}\tilde{z}, \quad (5)$$

$$M_{12} = M_{21} = -8\epsilon^2\tilde{P}\int_0^{\tilde{L}} g(\tilde{z})\mathcal{L}_{5,3}\mathrm{d}\tilde{z}, \quad (6)$$

$$\mathrm{V}_1 = -4\epsilon\theta_0\tilde{P}\int_0^{\tilde{L}} h(\tilde{z})\left[\tilde{z}\mathcal{L}_{3,2} - \epsilon\frac{\tilde{z}}{1+\tilde{z}^2}\mathcal{L}_{5,2}\right]\mathrm{d}\tilde{z}, \quad (7)$$

$$\mathrm{V}_2 = -4\epsilon\theta_0\tilde{P}\int_0^{\tilde{L}} h(\tilde{z})\left[\mathcal{L}_{3,2} + \epsilon\frac{\tilde{z}^2}{1+\tilde{z}^2}\mathcal{L}_{5,2}\right]\mathrm{d}\tilde{z}, \quad (8)$$

where we defined $\theta_0=w_0/z_0$ as the half-divergence of the beam and introduced the reduced coordinates, $\tilde{r}=r/w_0$ and $\tilde{z}=z/z_0$, and power, $\tilde{P}=P_0/P^*$, where $P_0=ncw_0^2E_0^2/16$ is the total input power and $P^*=cK/n$ ($\sim$mW) is a characteristic power with c the speed of light in free space. In addition, $f(\tilde{z})=\sin^2(\tilde{q}\tilde{z})/(1+\tilde{z}^2)$, $g(\tilde{z})=\tilde{z}(\tilde{z}^2-1)\sin^2(\tilde{q}\tilde{z})/(1+\tilde{z}^2)^3$, $h(\tilde{z})=\sin(\tilde{q}\tilde{z})/(1+\tilde{z}^2)^2$, and $\mathcal{L}_{n,m}=\frac{1}{2}\Gamma(n+1/2)[2/(1+\tilde{z}^2)+2(m-1)]^{-(n+1)/2}$ with Γ the Gamma function.

Typical light-induced elastic distortion patterns are shown in Fig. 2 for $w_0=1$ μm, $L=100$ μm, $n_\perp=1.53$, $n_\parallel=1.77$, and a reduced power $\tilde{P}=P_0/P^*=200$. The radial and azimuthal patterns are displayed in Figs. 2(c) and 2(d), respectively. Moreover, it is found that the handedness of the chiral azimuthal pattern, which is clearly identified in Fig. 2(b), is related to the incident CP handedness.

In experiments, we used the setup shown in Fig. 3.

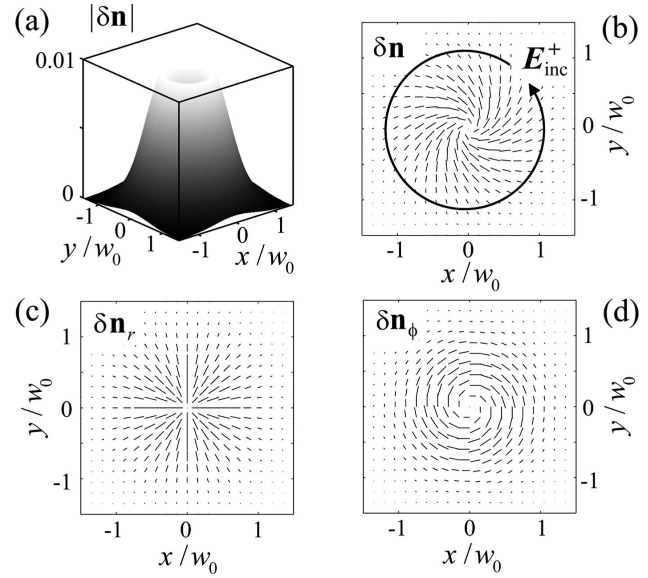

Fig. 2. Light-induced elastic distortion patterns: (a) Total amplitude, and (b) total, (c) radial, and (d) azimuthal transverse patterns at $z=L/2$ (see text for details).

A $\mathbf{c}_+$ polarized TEM_{00} pump beam with $\lambda_1=514.5$ nm is focused (half-filled NA=0.5 objective that gives a beam-waist diameter of ≈ 2 μm) at normal incidence on a $L=100$-μm-thick nematic LC film (E7, from Merck) with strong anchoring conditions that impose $\mathbf{n}=\mathbf{e}_z$ in the absence of light. The output $\mathbf{c}_\pm$ components are separated using a quarter-wave plate and a polarization beamsplitter and imaged on $\mathrm{CCD}_{1,2}$. Finally, a weak collinear linearly polarized TEM_{00} beam ($\lambda_2=632.8$ nm) probes the illuminated region, and its orthogonal linearly polarized output component is monitored by CCD_3.

At low incident power, the LC is almost unperturbed and the main features expected from a c-cut uniaxial crystal are observed [5,6], namely, the generation of a $\mathbf{c}_-$ polarized optical vortex associated with a phase singularity described by a phase factor $\exp(i\ell\phi)$ with $\ell=2$, as shown by the double spiral fringes obtained from interferences between the input and the $\ell=2$ beams [see inset of Fig. 3]. Conversely, the $\mathbf{c}_+$ polarized counterpart has a smooth wavefront profile and bears no orbital angular momentum ($\ell=0$). The corresponding doughnut and bell-shaped intensity patterns are shown in Fig. 4(a), and the optical axis distribution is evidenced by the so-called Maltese cross for the probe beam [a twisted version of it, see below, is shown in Fig. 4(c)].

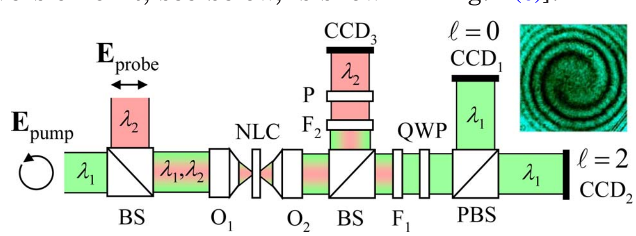

Fig. 3. (Color online) Experimental setup: BS, beam splitter; O_i, microscope objectives; NLC, nematic liquid crystal; F_i, interference filters; QWP, quarter-wave plate; PBS, polarization beam splitter; P, polarizer. Inset, spiraling fringe patterns (see text for details).

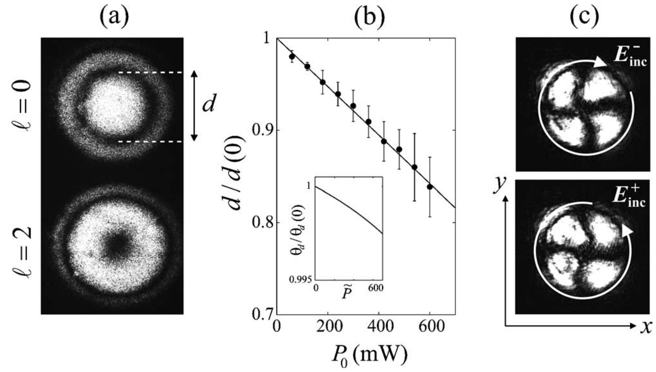

Fig. 4. (a) $\mathbf{c}_\pm$ components of the output pump beam associated with $\ell=0,2$. (b) Dislocation ring diameter of the $\ell=0$ output pump beam component versus input power. (c) Output probe beam for $\mathbf{c}_\pm$ incident pump beam. Inset, angle θ_d associated with the first dislocation ring versus power.

As the power is increased, cylindrically symmetric light-induced elastic distortions build up and are retrieved from the $\mathbf{c}_\pm$ output intensity patterns for the pump beam. This is illustrated in Fig. 4(b), where the power dependence of the first dislocation ring diameter, d, measured from the $\ell=0$ component [Fig. 4(a)], is shown. This dark ring corresponds to a π total phase delay between extraordinary and ordinary waves. Hence, we conclude that the larger is the power, the larger is the effective birefringence for that particular direction given by the angle θ_d. The latter angle is thus defined from $\pi \simeq (2\pi/\lambda)\int_0^L \Delta n_{\rm eff}(r=\theta_d z,z)\mathrm{d}z$, where $\Delta n_{\rm eff}(r,z)\simeq n\epsilon\theta_{\rm eff}^2(r,z)$ is the effective birefringence with $\theta_{\rm eff}(r,z)\simeq\theta_d+|\delta\mathbf{n}|(r,z)$ the local angle between the director and the optical ray at an angle θ_d from the z axis. The predicted power dependence of θ_d is shown in the inset of Fig. 4(b), which offers a qualitative agreement only. This is explained by the crude, single-mode approximation ($M=1$) that implies a symmetric longitudinal distortion profile although the optical torque density is longitudinally asymmetric in practice. This could be taken into account by retaining higher-order modes ($M>1$) but without change of the overall qualitative behavior. The above observations prove the appearance of radial elastic distortions, $\delta n_r(r,z)\neq 0$, and the null intensity at $r=0$ for the $\ell=2$ beam allows to precise that $\delta n(r=0,z)=0$. Moreover, the Maltese cross is all the more twisted as the power is increased (not shown here), which is the signature of power-dependent azimuthal distortions, $\delta n_\phi(r,z)\neq 0$. Finally, we find that the handedness of such chiral pattern depends on the incident input polarization handedness; see Fig. 4(c). A qualitative overall agreement with the model is therefore obtained until the axial symmetry breaks down at a higher power through an orientational Fréedericksz instability.

Mechanical effects of CP light in axially symmetric, but inhomogeneous, LCs have been recently discussed for radial nematic droplets [17,18]. In [17] the dielectric torque density was shown to locally balance the moment of the optical radiation force density. The laser-induced distortions issues, however, were not considered, and the calculations were done using an erroneous representation of the electric field, free of phase singularity. Nevertheless, the use of a correct representation leaves the conclusions of [17] unchanged. In contrast, [18] reports on light-induced chiral distortions, however, neither unveiling the physical mechanism at work nor giving a quantitative description of the phenomenon.

In conclusion, we have demonstrated that nonsingular light beams can generate singular birefringent patterns in homogeneous uniaxial elastic media. Radial and spin-dependent azimuthal laser-induced distortion modes have been theoretically predicted and experimentally observed in LC thin films.

I. Jánossy is acknowledged for communication of [17] prior to publication and R. Wunenburger for careful reading of the manuscript and discussions.

References

1. L. Allen, S. M. Barnet, and M. J. Padgett, *Optical Angular Momentum* (IoP Publishing, 2003).
2. T. A. Nieminen, A. B. Stilgoe, N. R. Heckenberg, and H. Rubinsztein-Dunlop, J. Opt. A, Pure Appl. Opt. **10**, 115005 (2008).
3. V. S. Liberman and B. Y. Zeldovich, Phys. Rev. A **46**, 5199 (1992).
4. C. Schwartz and A. Dogariu, Opt. Express **14**, 8425 (2006).
5. A. Ciattoni, G. Cincotti, and C. Palma, J. Opt. Soc. Am. A **20**, 163 (2003).
6. A. Volyar and T. Fadeyeva, Opt. Spectrosc. **94**, 235 (2003).
7. A. Niv, G. Biener, V. Kleiner, and E. Hasman, Opt. Commun. **251**, 306 (2005).
8. L. Marrucci, C. Manzo, and D. Paparo, Phys. Rev. Lett. **96**, 163905 (2006).
9. Y. Gorodetski, A. Niv, V. Kleiner, and E. Hasman, Phys. Rev. Lett. **101**, 043903 (2008).
10. S. C. McEldowney, D. M. Shemo, R. A. Chipman, and P. K. Smith, Opt. Lett. **33**, 134 (2008).
11. H. Ren, Y.-H. Lin, and S.-T. Wu, Appl. Phys. Lett. **89**, 051114 (2006).
12. N. V. Tabiryan, A. V. Sukhov, and B. Ya. Zel'dovich, Mol. Cryst. Liq. Cryst. **136**, 1 (1986).
13. A. Ciattoni, B. Crosignani, and P. Di Porto, J. Opt. Soc. Am. A **18**, 1656 (2001).
14. E. Brasselet, Y. Izdebskaya, V. Shvedov, A. S. Desyatnikov, W. Krolikowski, and Y. S. Kivshar, Opt. Lett. **34**, 1021 (2009).
15. Z. Bomzon, M. Gu, and J. Shamir, Appl. Phys. Lett. **89**, 241104 (2006).
16. Y. Zhao, J. S. Edgar, G. D. M. Jeffries, D. McGloin, and D. T. Chiu, Phys. Rev. Lett. **99**, 073901 (2007).
17. I. Jánossy, Opt. Lett. **33**, 2371 (2008).
18. E. Brasselet, N. Murazawa, S. Juodkazis, and H. Misawa, Phys. Rev. E **77**, 041704 (2008).